RESEARCH REPORT

VTT-R-00211-20

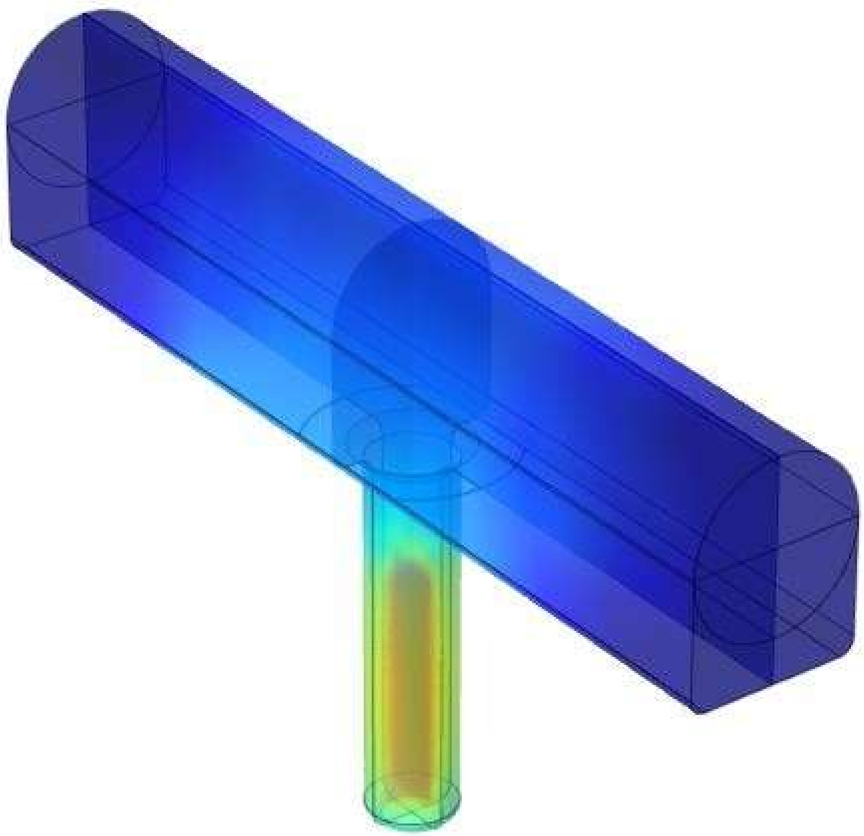

Thermal evolution and thermally induced stress simulations of spent nuclear fuel repository

Author: Sami Naumer

Confidentiality: Public

VTT

Report's title	
Thermal evolution and thermally induced stress simulations of spent nuclear fuel repository	
Customer, contact person, address Finnish Research Programme on Nuclear Waste Management KYT2022	**Order reference**
Project name Bentonite-rock interaction	**Project number/Short name** 122442/ KYT2022_BROCTIO
Author(s) Sami Naumer	**Pages** 35
Keywords Spent nuclear fuel, geological, repository, decay heat, temperature, thermal stress, damage analysis	**Report identification code** VTT-R-00211-20

Summary

In this study, a COMSOL Multiphysics model was created to analyze 1) the heat transfer and 2) the thermal expansion induced stresses in Olkiluoto spent nuclear fuel repository. The temperature field of the near disposal hole area was calculated and the minimum disposal hole spacing for 25 m tunnel spacing was analyzed. With 95 °C maximum allowed temperature in bentonite buffer, the minimum spacing was 8.845 m. The results were verified by comparing them to the results by Ikonen, et al. (2018). The verification showed that the results are very close to previous simulations with the difference in the maximum temperature being less than 0.1 °C.

In the second phase, the temperature field was used to analyze the thermally induced stress in the rock around the disposal hole. The study resulted in a maximal increase in shear stress of 83.7 MPa in the sharp corners of the tunnel floor. The damage caused by the stress was analyzed using different failure criterions and the analysis showed that the damage mainly occurs in the disposal hole walls.

Confidentiality	Public

Espoo 27.2.2020

Written by	**Reviewed by**	**Accepted by**
Sami Naumer, Research trainee	Veli-Matti Pulkkanen Research scientist	Suvi Karvonen Research team leader

VTT's contact address
sami.naumer@vtt.fi

Distribution (customer and VTT)
KYT2022 Programme

Preface

This study was conducted at VTT and it was financed by KYT2022 project BROCTIO and EC EURAD WP HITEC.

I would like to thank my supervisor Veli-Matti Pulkkanen who guided me through this study and helped me not only with the model but also to really understand the phenomenon behind it. I would also like to thank Juha Kuutti who gave me insight to the earlier study of the disposal area.

Contents

1. Introduction

1.1 Background

In Finland spent nuclear fuel (SNF) is planned to be disposed in a deep geological repository in Olkiluoto (Figure 1). The SNF is placed in cast iron inserts into copper canisters (SNF-canister) in a fuel encapsulation plant on the surface. The SNF-canisters are transported to the disposal level at the depth of 420 m and brought into disposal tunnels, where they are emplaced into vertical boreholes in the tunnel floor. The canister is then surrounded with bentonite clay and the tunnel is backfilled with clay (Saanio, et al., 2013). In total 9 Mt of SNF is planned to be disposed at the site. The number includes SNF from all current nuclear reactors and SNF from the Olkiluoto 3 in the future (Saanio, et al., 2013). The planned disposal rate is 122 canisters per year (Ikonen, et al., 2018).

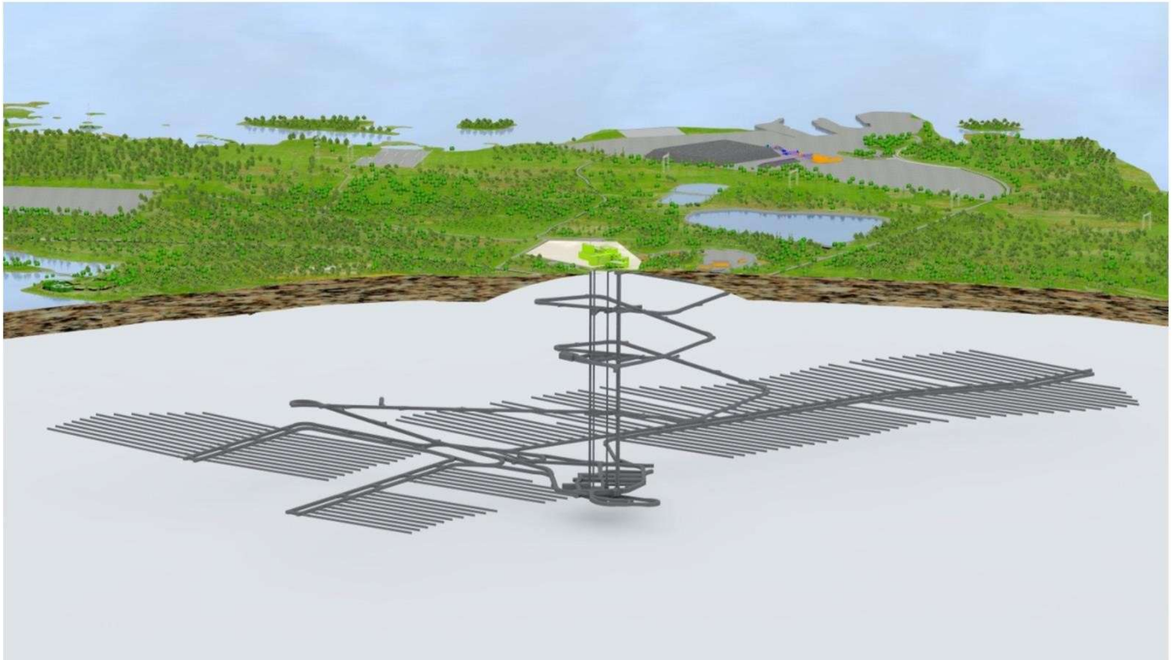

Figure 1. *A schematic plan for the deep geological repository at Olkiluoto. Posiva Oy*

According to Posiva's Safety Case, the bentonite buffer and the tunnel backfill have multiple safety functions (e.g. Juvankoski 2013). One main function is to slow down transport of radionuclides. Bentonite is a type of clay that swells when exposed to water. The swelling prevents water flow through the buffer and makes transport of radionuclides slow in a case of a canister failure. Other main functions are protection of the SNF-canister from mechanical damage as well as chemical and biological processes that could damage the canister.

The SNF consists of a mixture of radionuclides, which continue radioactive decay after the fuel is taken out from the nuclear reactors. The heat produced by the decay causes the SNF-canister to heat up. For final disposal, the allowed maximum heat power for BWR-fuel canisters is 1700 W (Raiko, 2013). This power is achieved by cooling the spent nuclear fuel before disposal. The time needed for cooling depends on the fuel burn-up (Ikonen, 2005). The fuel burn-up describes the relation between produced heat energy of the nuclear fuel compared to the mass of the fuel (Ikäheimonen, 2002). The SNF-canister heats up the surrounding bentonite pellets and blocks from where the heat diffuses to the surrounding rock (Juvankoski, 2013).

The bentonite blocks should not exceed 100 °C to preserve bentonite's material properties. There are, however, uncertainties in material properties such as heat conductivity and heat capacity. Because of the uncertainties, a safety margin is used to ensure that the bentonite will not overheat (Ikonen & Raiko, 2012). A safety margin of 5 °C is chosen meaning that the temperature of the disposal canisters should not exceed 95 °C. The reasoning behind the safety margin is discussed in detail by Ikonen, et al. (2018). If the canister heat power is fixed and the material properties are not changed, the most important variable that determines the temperature between the disposal holes is the distance between them. Thermal analysis about the spacing between disposal holes has been previously conducted by Ikonen & Raiko (2012) and Ikonen, et al. (2018) using VTT in-house code and Abaqus.

The rock massif, where the SNF-disposal takes place is under an initial in situ stress. When the tunnels have been excavated, the in situ stress causes a load on the underground structure and has to be taken into account in the site design (Brady & Brown, 2006). The excavation causes the stress to distribute around the openings. If the stress in the underground structures exceeds a certain failure criterion discontinuities will form in the rock. The discontinuities can appear for example as fractures or spalling. These failures can cause damages to the surrounding rock material and the tunnels. The heat of the SNF-causes the host rock to heat up and expand which induces an additional thermal stress in it. The thermally induced stress has been studied previously by Hakala (2014) and Valli (2014).

1.2 Objectives and scope

The objectives of this study are:

1. to implement a COMSOL Multiphysics heat transfer model to analyze temperature in the disposal site.
2. to verify the implementation by comparing the to those by Ikonen, et al. (2018).
3. to use the thermal model to assess the effect of thermal expansion on rock stability in the disposal site and compare the results to previous studies by Hakala (2014) and Valli (2014).

In the future the verified model can be utilized in 1) scoping the thermal conditions of the disposal site for experiments and 2) in developing thermally coupled models with a flexible simulation software.

The study is limited by the following factors:

1. Only canisters containing Finnish boiling water reactor (BWR) SNF from Olkiluoto nuclear power plant OL1 and OL2 reactors is analyzed.
2. In the thermal analyses (apart from the verification -study), it is assumed that the analyzed disposal canister is in the middle of an infinite panel of deposition holes and all the canisters are disposed simultaneously.
3. In the rock mechanics analyses, only a small volume of rock surrounding the disposal hole is studied and the effect of other disposal tunnels is neglected.
4. The effect of water pressure on rock mechanics is not considered in the simulations.

1.3 Studied tasks

1.3.1 Task 1 and Task 2

Task 1 is conducted to verify the results obtained with the developed COMSOL Multiphysics model by comparing the results to the earlier study by Ikonen, et al. (2018). They verified the results of a VTT in-house control volume based calculation by comparing the results with the commercial software Abaqus. In Task 1, the same model is recreated with COMSOL Multiphysics and the results of all three models are compared.

The simulations are also run with a different host rock heat conductivity presented in the study of Kukkonen (2015) to see if the difference in the results between these models are significant in comparison to the uncertainties in rock heat conductivity.

In Task 2, the thermal effect of the decay heat of the SNF-canisters to the surrounding buffer and host rock material is calculated. The task uses geometric dimensions and material properties similar to Ikonen, et al. (2018) but also other sources are used when there is uncertainty in the data. Task 2 also takes into account the disposal tunnel, whereas the study of Ikonen, et al. (2018) does not. The calculations are conducted for disposal hole spacing ranging from 6 m to 20 m and tunnel spacing of 25 m, 30 m, 35 m and 40 m. The minimum disposal hole spacing such that the maximum temperature on bentonite surface does not exceed 95 °C is evaluated for tunnel spacing of 25 m. Finally, a more accurate way (than by Ikonen, et al. 2018) to take radiative heat transfer into account in the gap between the copper over pack and the cast insert is tested to see its effect on the results. Minimizing the distance between the disposal holes without exceeding the temperature limit is of interest as with longer distances between the holes longer tunnels will have to be built. Reducing the need for tunnel excavation and backfill materials has a smaller ecological footprint and is more cost effective.

1.3.2 Task 3

The aim of Task 3 is to see how the thermal expansion of the rock affects the stress state in it. If the stress exceeds the strength of the rock, discontinuities may form in it. This is important to study because increased amount of fractures in the host rock affect the radionuclide transport in case of a canister leakage (Poteri, et al., 2014). Fractures might also affect the thermal properties of the rock along with structural strength.

A study on thermally induced rock stress increment has been conducted by Hakala et al. (2014). The study takes the whole disposal faculty into account. In Task 3 however, the focus is on a section of a disposal tunnel that has been used in the thermal model in Task 2.

Task 3 is divided to two parts. In the first part, the bentonite is assumed to be fully water saturated. The rock is under in-situ stresses and additionally the saturated bentonite causes an 5 MPa boundary load on the tunnel and disposal hole walls. The geometry is a section of a disposal tunnel that is extracted from the host rock and filled with wet bentonite. The first part is used as a reference for the results of the second part. In addition to bentonite swelling stress the second part takes into account the thermally induced stress in the studied area. This is carried out by importing the temperature field from Task 2.

The temperature data of Task 2 with the minimal disposal hole spacing is used in this analysis. The internal details of the copper canister are not needed as the temperature field of the surrounding rock can be imported from Task 2.

2. Model Geometry

The purpose of this chapter is to represent the spatial dimensions needed for the simulations in this study. The base on the spatial dimensions is on Ikonen, et al. (2018) and the missing data is filled based on other studies. All the dimensions are for the complete three-dimensional model. In the model however, symmetry in the y- and x-axis is used for decreasing the need for computational resources.

2.1 The host rock

The host rock is modelled as a three dimensional block. In Task 1, the block is 100 m wide, 100 m long and 200 m tall.

In Task 2, the dimensions for the host rock are as follows: The width of the block is defined by the tunnel spacing (25 m, 30 m, 35 m and 40 m). The length of the block is the length between disposal holes and is varied ranging from 6 m to 20 m. The height of the block should be sufficiently tall so that the thermal pulse of the disposal canister does not reach the surface or bottom on the time scale of the study. The height is set to 200 m and the disposal tunnel is situated in the middle.

In Task 3, an area consisting of one disposal tunnel with one disposal hole is modelled. The dimension for the host rock block are chosen so that the tunnel and disposal hole fits inside. The dimensions of study 3 for the host rock block are 20 m x 20 m x 20 m. The dimensions of the host rock block from all three studies are presented in Table 1.

According to Saanio, et al. (2013) the tunnel has a total height of 4 400 mm from which the lower part is 2 650 mm tall (Figure 2.). The roof part of the tunnel is a semicircle with a radius of 1 750 mm. The tunnel is 3 500 mm wide. The disposal hole has a diameter of 1 750 mm and a depth of 7 787 mm (Table 2). The disposal hole is located so that its top is in the middle of the host rock block.

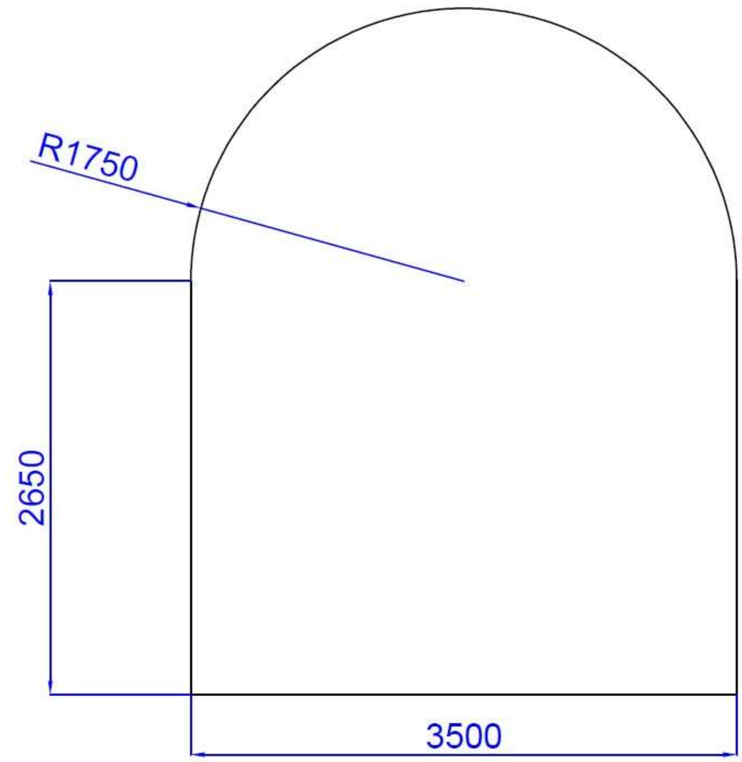

Figure 2. *Tunnel profile dimensions in mm.* (Ikonen, et al., 2018)

Table 1. *Host rock dimensions in Task 1, Task 2 and Task 3 in m.*

Task	Width	Length	Height
Task 1	100	100	200
Task 2	25, 30, 35, 40	6 - 20	200
Task 3	20	20	20

Table 2. *Tunnel and disposal hole dimensions in mm.*

Part	Dimension	Source
Tunnel width	3 500	(Keto, et al., 2013)
Tunnel bottom height	2 650	(Keto, et al., 2013)
Tunnel total height	4 400	(Keto, et al., 2013)
Tunnel ceiling radius	1 750	(Keto, et al., 2013)
Hole depth	7 787	(Ikonen, et al., 2018)
Hole diameter	1 750	(Ikonen, et al., 2018)

2.2 The bentonite buffer

According to Juvankoski (2013), the disposal canister is surrounded by bentonite blocks. Below the canister lies the disk-shaped bottom block. Disk blocks with a hole in the middle, the ring blocks, surround the canister. Above the canister are multiple disk-shaped blocks, but for the purpose of this model, they are modelled as one single cylindrical block. The dimensions for the bentonite blocks are presented by Ikonen, et al. (2018) and listed in Table 3. The dimensions are also presented in Figure 3 along with canister dimensions.

Table 3. *Bentonite buffer dimensions in mm.*

Part	Dimension	Source
Bottom block height	500	(Ikonen, et al., 2018)
Bottom block radius	807.5	(Ikonen, et al., 2018)
Ring block outer radius	825	(Ikonen, et al., 2018)
Ring block inner radius	560	(Ikonen, et al., 2018)
Ring block height	4777	(Ikonen, et al., 2018)
top block height	2510	(Ikonen, et al., 2018)
Top block radius	807.5	(Ikonen, et al., 2018)

Bentonite pellets fill the empty space around the canister and the outer gap between the bentonite blocks and the disposal hole. Additionally the space between the copper canister collars and the top blocks are filled with pellets. All the pellet filling dimensions are presented in Table 4.

The outer pellet gap is 67.5 mm wide above and below the canister. That part is 2 510 mm tall over the canister and 500 mm tall under the canister. Next to the canister, the gap is 50 mm wide. The inner pellet gap is 35 mm wide and 4 777 mm tall. That part is 4 777 mm tall. The filling adjacent to the copper collars consists of two cylinders. The bottom one has a radius of 425 mm and the top cylinder a radius of 410.5 mm. The bottom cylinder is 50 mm tall and the upper one 35 mm. (Ikonen, et al., 2018)

Table 4. *Pellet filling dimensions in mm.*

Part	Dimension	Source
Outer gap width at canister	50	(Ikonen, et al., 2018)
Height at canister	4 777	(Ikonen, et al., 2018)
Outer gap width over and under the canister	67.5	(Ikonen, et al., 2018)
Height of the outer gap over canister	2 510	(Ikonen, et al., 2018)
Height of the outer gap under the canister	500	(Ikonen, et al., 2018)
Inner gap width	35	(Ikonen, et al., 2018)
Inner gap height	4 777	(Ikonen, et al., 2018)
Collar filling bottom radius	425	(Ikonen, et al., 2018)
Collar filling bottom height	50	(Ikonen, et al., 2018)
Collar filling top radius	410.5	(Ikonen, et al., 2018)
Collar filling top height	35	(Ikonen, et al., 2018)

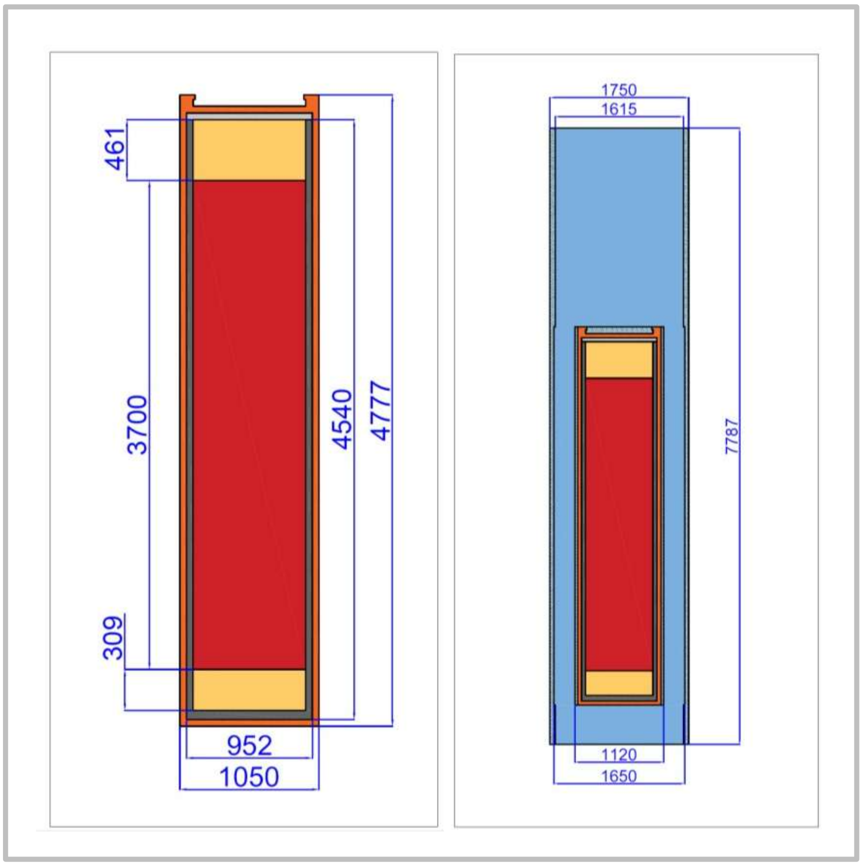

Figure 3. *Dimensions of the SNF-canister and buffer in millimetres.*

2.3 The canister

For the cast insert, similar geometry is used as in Figure 2 in (Ikonen, et al*.,* 2018). The copper canister dimensions are presented in Table 5, the canister details in Table 6 and the cast insert dimensions in Table 7. Figure 3 shows the canister dimensions and Figure 4 the canister details. The canister has a narrow argon filled gap between the copper over pack and the cast insert.

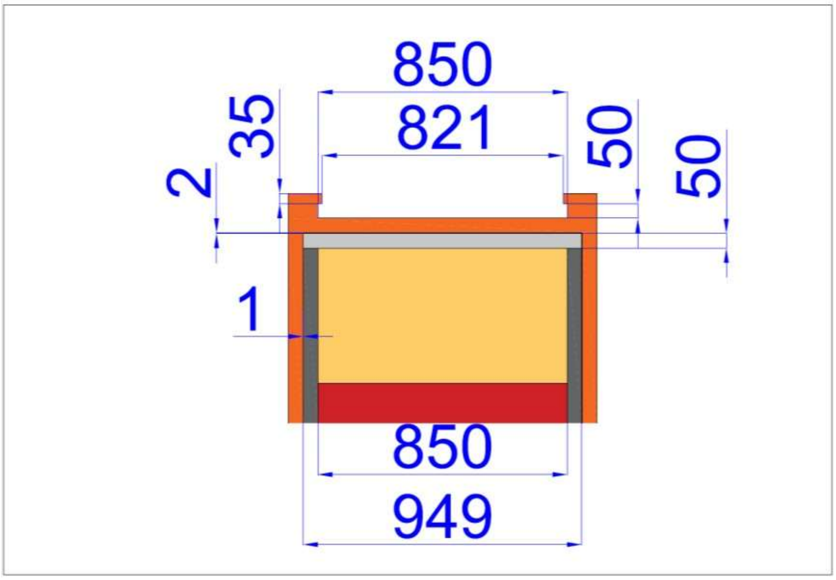

Figure 4. *Dimensions of the copper canister and cast insert details in millimetres.*

Table 5. *Dimensions of the copper canister in mm.*

Parameter	Dimension	Source
Total length	4777	(Ikonen, et al., 2018)
Inside length	4592	(Ikonen, et al., 2018)
Outer diameter	1050	(Ikonen, et al., 2018)
Inner diameter	952	(Ikonen, et al., 2018)

Table 6. *Details of the copper canister in mm.*

Parameter	Dimension	Source
Bottom thickness	50	(Ikonen, et al., 2018)
Top thickness	50	(Ikonen, et al., 2018)
Collar lower space height	50	(Ikonen, et al., 2018)
Collar lower space diameter	850	(Ikonen, et al., 2018)
Collar upper part height	35	(Ikonen, et al., 2018)
Collar upper part diameter	821	(Ikonen, et al., 2018)

In the model by Ikonen et al. (2018), the cast insert model geometry is simplified such, that the steel lid lies on top of the insert. The fuel rods and the inner parts of the cast insert are simplified to a homogenized cylinder. This cylinder is split to three parts. The heat generating part is in the middle and no heat generating parts above and below it. The outer part of the cast insert surrounds the cylinder. The homogenized cylinder details are presented in Table 8. The cast insert details are presented in Table 7 and the steel lid details in Table 9. Similar geometry is used in the COMSOL model here, but the diameter of the homogenized cylinder is slightly thicker in the COMSOL model than in the model by Ikonen et al. (2018). The thickness of the cast insert and the diameter of the homogenized cylinder of the VTT in-house model (Ikonen, et al., 2018) are presented in brackets behind the COMSOL model values in Table 7.

Table 7. *Cast insert dimensions in mm.*

Parameter	Dimension	Source
Total length	4540	Calculated from (Ikonen, et al., 2018)
Inside length	4470	(Ikonen, et al., 2018)
Diameter	949	(Ikonen, et al., 2018)
Bottom thickness	70	(Ikonen, et al., 2018)
Wall thickness	49.5 (33)	(Ikonen, et al., 2018)

Table 8. *Homogenized cylinder dimensions in mm. The diameter of the homogenized cylinder by Ikonen, et al. (2018) is in brackets.*

Parameter	Dimension	Source
Diameter	850 (883)	(Ikonen, et al., 2018)
Heat generating part length	3650	(Ikonen, et al., 2018)
Length above heat generating part	461	(Ikonen, et al., 2018)
Length below heat generating part	309	(Ikonen, et al., 2018)

Table 9. *Steel lid dimensions in mm.*

Parameter	Dimension	Source
Lid thickness	50	(Raiko, 2005)
Diameter radius	910	(Raiko, 2005)

3. Mathematical model

3.1 Heat transfer in solids

The energy balance equation for heat transfer in solids can be written as:

$$\rho C_{\mathrm{p}} \frac{\partial T}{\partial t} + \nabla \cdot (\boldsymbol{q} + \boldsymbol{q}_{\mathbf{r}}) = Q, \tag{1}$$

where ρ is the density of the material further explained in Section 4.1.1. C_p is the specific heat capacity of the material further explained in Section 4.1.2. T is the temperature and Q stands for volumetric heat sources. In this study, the disposal canister is treated as a heat source. $\boldsymbol{q}$ is the heat transferred by conduction expressed by Fourier's law:

$$\boldsymbol{q} = -\lambda \nabla T, \tag{2}$$

where λ is the heat conductivity of the material further explained in Section 4.1.3. $\boldsymbol{q}_{\mathbf{r}}$ is the heat transferred with radiation.

For the first part of Task 2, the radiative heat transfer is included in the effective heat conductivity of the radiation gap. Thereby the term $\boldsymbol{q}_{\mathbf{r}}$ is omitted. The heat transfer equation without the radiative heat transfer is expressed as equation:

$$\rho C_{\mathrm{p}} \frac{\partial T}{\partial t} + \nabla \cdot q = Q. \tag{3}$$

The heat flux is now $\boldsymbol{q} = -\lambda_{\mathrm{eff}} \nabla T$, where λ_{eff} is the effective heat conductivity. The radiative heat transfer is modelled more accurately in the second part of Task 2. The radiative heat transfer is further discussed in Section 3.2.

3.2 Radiation over argon gap

In the second part of Task 2, the surface-to-surface radiation module in COMSOL Multiphysics is coupled with the heat transfer in solids module to see if a more accurate model for the radiation affects the minimum tunnel distance. The surface-to-surface radiation module can be used to simulate heat transfer via radiation with various fidelities. In the model here. all surfaces (the copper canister surface, the cast iron surface and the steel lid surface) are set as opaque, such that no radiation goes through them. The boundaries are modelled as ideal grey bodies. For them the inward radiative heat flux is given by

$$\boldsymbol{q}_{\mathbf{r}} = \varepsilon (G - n^2 e_{\mathrm{b}}(T)) \boldsymbol{n} \tag{4}$$

where ε is the surface emissivity of the surface material, G the total incoming radiative flux from other radiation boundaries in the model, n the refractive index of the surface material. $e_b(T)$ the power radiated by the surface material on all wavelengths (COMSOL, 2018) and $\boldsymbol{n}$ the surface normal. According to the Stefan-Bolzmann law,

$$e_{\mathrm{b}}(\mathrm{T}) = \sigma T^4 , \tag{5}$$

where σ is the constant of proportionality and T the temperature of the surface.

3.3 Solid mechanics

In Task 3, the effects of the heat on the surrounding rock are studied. The temperature field computed in Task 2 is used. The simplifications for the model are as follows:

1. The material is assumed linear elastic and isotropic.
2. The host rock fractures are not taken into account.
3. Groundwater pressure effect on the mechanical behaviour of the rock is not taken into account.
4. Effects of gravity are omitted.

In a stationary case, the force balance equation

$$\nabla \cdot \boldsymbol{\sigma} = 0 \tag{6}$$

is solved. Here $\boldsymbol{\sigma}$ is the Cauchy stress tensor. The material behavior is determined by the linear stress-strain relation

$$\boldsymbol{\sigma} = \boldsymbol{\sigma}_{\text{ext}} + \frac{E}{(1+v)}\boldsymbol{\varepsilon}_{\text{el}} + \frac{E}{(1+v)(1-2v)} tr(\boldsymbol{\epsilon}_{\text{el}})\boldsymbol{I}, \tag{7}$$

where $\boldsymbol{\epsilon}_{\text{el}}$ is the elastic strain tensor and $\boldsymbol{\sigma}_{\text{ext}}$ is the external stress tensor further explained in Chapter 4.3.1, *E* is the Young's modulus and v is the Poisson's ratio. The elastic strain $\boldsymbol{\varepsilon}_{\text{el}}$ is the difference between the total strain $\boldsymbol{\varepsilon}$

$$\boldsymbol{\varepsilon} = \frac{1}{2}[(\nabla \boldsymbol{u})^T + \nabla \boldsymbol{u}] \tag{8}$$

where $\boldsymbol{u}$ is the total displacement, and the inelastic strain $\boldsymbol{\varepsilon}_{\text{inel}}$:

$$\boldsymbol{\varepsilon}_{\text{el}} = \boldsymbol{\varepsilon} - \boldsymbol{\varepsilon}_{\text{inel}} \tag{9}$$

In the model here, the inelastic strain is the thermal strain, $\boldsymbol{\varepsilon}_{\mathbf{th}}$:

$$\boldsymbol{\varepsilon}_{\text{inel}} = \boldsymbol{\varepsilon}_{\text{th}} = \alpha(T)(T - T_{\text{ref}})\boldsymbol{I} \tag{10}$$

where α is the coefficient of thermal expansion and T_{ref} the initial temperature.

3.3.1 Failure criterion

For determining the strength of the rock in the repository, a Drucker-Prager failure criterion is used. If the failure criterion is exceeded, fractures and other discontinuities start to form in the rock. The Drucker-Prager criterion is expressed by equation (e.g. (Bocci, 2014) and (Alejano & Bobet, 2012)):

$$\sqrt{J_2} - \frac{2}{\sqrt{3}} \cdot \frac{\sin(\phi)}{3 - \sin(\phi)} \cdot I_1 + \frac{2\sqrt{3}\, c \cdot \cos(\phi)}{3 - \sin(\phi)} = 0 \tag{11}$$

Here, J_2 is the second invariant of the stress deviator tensor, I_1 the first invariant of the effective stress tensor, *c* the cohesion and ϕ the internal angle of friction. The parameters for the failure criterion in both Posiva (2012) and Siren (2011) are for Mohr Coulomb failure criterion. The parameters are compatible with Drucker-Prager failure criterion and the relationship has been taken into account in Equation 12. J_2 and I_1 can be calculated from the principal stresses σ_1, σ_2 and σ_3 as follows:

$$J_2 = \frac{1}{6}\,[(\sigma_1 - \sigma_2)^2 + (\sigma_1 - \sigma_3)^2 + (\sigma_3 - \sigma_1)^2] \quad (12)$$

$$I_1 = \sigma_1 + \sigma_2 + \sigma_3 \quad (13)$$

4. Model parameters

4.1 Task 1 and Task 2

4.1.1 Density

The densities of the materials used in the model are presented in Table 2. According to Kukkonen (2015) the average density of the host rock is 2712 kg/m^3. In the report by Ikonen et al. (2018) no density for the bentonite blocks and pellets is given thus following values by Hökmark, et al. (2009) and Juvankoski (2013) are used. According to Hökmark et al. (2009), the dry density of the bentonite pellets is 1100 kg/m^3. Juvankoski (2013) states different bulk densities for both the ring blocks and disk blocks. 2000 kg/m^3 is however used in this study and will be sufficient for this analysis, as the difference between the densities is small. The backfill is modelled as a homogenized material and the dry density is calculated as an average of all of its components presented in Table 10, with the equation (Keto, et al., 2013):

$$\frac{\sum_{i=1}^{n} \rho_i \cdot V_i}{V_i} \tag{14}$$

Table 10. *Backfill material parameters.*

Parameter	Blocks	Pellets	Foundation
volume [m^3]	12.11	2.93	1.39
density [kg/m^3]	2030	1000	1250

With the parameters from Table 10, the average density of the backfill material can be calculated using Equation 14.

$$\frac{2030\ \frac{kg}{m^3} * 12.11\ m^3 + 1000\ \frac{kg}{m^3} * 2.93\ \ m^3 + 1250\ \frac{kg}{m^3} * 1.39\ \ m^3}{12.11\ \ m^3 + 2{,}93\ \ m^3 + 1.39\ \ m^3} = 1783\ \frac{kg}{m^3}$$

The densities for the copper cylinder, cast insert and steel lid are presented by Raiko (2013). For the argon gas, a value of 1.661 kg/m^3 in normal temperature and pressure (20 °C and 1 atm) is used (Engineering ToolBox, 2003). The densities of rest of the materials are presented in Table 11.

Table 11. *Densities of the used materials in kg/m^3.*

Backfill material		
Backfill dry density in initial conditions	1783	(Keto, et al., 2013)
Backfill dry density in saturated conditions	1758	(Keto, et al., 2013)
Buffer material		
Bentonite block bulk density	2000	(Juvankoski, 2013)
Bentonite pellet dry density	1100	(Hökmark, et al., 2009)
Host rock		
Rock density	2712	(Kukkonen, 2015)
Canister materials		
Copper density	8940	(Raiko, 2013)
Cast insert density	7200	(Raiko, 2013)
Steel lid density	7850	(Raiko, 2013)
Argon gas density	1.661	(Engineering ToolBox, 2003)

4.1.2 Specific heat capacity

In the study of Ikonen, et al. (2018) the volumetric heat capacity C_{V} is used for the host rock and the buffer materials. Volumetric heat capacity is also used for the backfill material by Ikonen and Raiko (2012). In COMSOL model, the specific heat capacity C_{p} is used so the values have to be calculated with

$$C_{\mathrm{p}} = \frac{C_{\mathrm{V}}}{\rho}. \tag{15}$$

The volumetric heat capacities are presented in Table 12.

Table 12. *Volumetric heat capacities of the materials in MJ/(m³·K).*

Host rock		
Volumetric heat capacity at 25 °C	2.11	(Ikonen, et al., 2018)
Volumetric heat capacity at 60 °C	2.25	(Ikonen, et al., 2018)
Buffer		
Bentonite block volumetric heat capacity	2.92	(Ikonen, et al., 2018)
Pellet volumetric heat capacity	1.58	(Ikonen, et al., 2018)
Backfill material		
Backfill volumetric heat capacity	1.75	(Ikonen & Raiko, 2012)

The specific heat capacities are presented in Table 13. The materials apart from the host rock have a constant heat capacity (not dependent on temperature). Specific heat capacities for the canister materials are presented by Raiko (2013). For the specific heat capacity of the host rock a linear approximation is used (Ikonen, et al., 2018)

$$c_{\mathrm{p}} = \frac{0.14\ MJ/(m\cdot K)/35\ ^{\circ}\mathrm{C}}{\rho} \cdot (T - 25\ ^{\circ}\mathrm{C}) + c_{\mathrm{p25\ ^{\circ}C}}, \tag{16}$$

where $c_{\mathrm{p25\ ^{\circ}C}}$ is the specific heat capacity of the rock at 25 °C.

Table 13. *Specific heat capacities of the used materials J/(kg·K).*

Host rock		
Specific heat capacity at 25 °C	778	calculated, Equation 5.
Specific heat capacity at 60 °C	829	calculated, Equation 5.
Buffer		
Bentonite block specific heat capacity	1460	calculated, Equation 5.
Pellet specific heat capacity	1436	calculated, Equation 5.
Backfill material		
Backfill specific heat capacity	981	calculated, Equation 5.
Canister materials		
Copper specific heat capacity	394	(Raiko, 2013)
Steel lid specific heat capacity	500	(Raiko, 2013)
Cast insert specific heat capacity	461	(Raiko, 2013)
Argon gas specific heat capacity	0.52	Calculated from Ikonen et al. (2018)

4.1.3 Heat conductivity

The third parameter is the thermal conductivity. The thermal conductivity parameters of the materials are presented in Table 15. The thermal conductivity of the host rock is temperature dependent and a linear approximation is used (Ikonen, et al., 2018):

$$\lambda = \frac{-0.05\frac{W}{m\cdot K}}{35^{\circ}\mathrm{C}} \cdot (T - 25\ ^{\circ}\mathrm{C}) + \lambda_{25\ ^{\circ}\mathrm{C}}. \tag{17}$$

Where $\lambda_{25\,°C}$ is the thermal conductivity of the host rock at 25 °C. In the study of Ikonen, et al. (2018) the heat transfer over the argon gap is a sum of radiative and conductive heat transfer. With applying an effective conductivity for the argon gap both forms of heat transfer are taken into account. The effective thermal conductivity is calculated with the following equation (Ikonen, et al., 2018):

$$\lambda_{\text{eff}}(T_{\text{mean}}) = \lambda_{\text{gas}}(T_{\text{mean}}) + 4\delta_{\text{local}}\,\varepsilon_{\text{tot}}\,\sigma T_{\text{mean}}^3. \quad (18)$$

Here, T_{mean} is the mean temperature in the argon gap, δ_{local} is the width of the gap. $\delta_{\text{local}} =$ 1.5 mm is used for both the radial and vertical gap. σ is the Stefan-Bolzmann constant and ε_{tot} is the total emissivity that can be calculated as:

$$\varepsilon_{\text{tot}} = \frac{\varepsilon_1\varepsilon_2}{\varepsilon_1+\varepsilon_2-\varepsilon_1\varepsilon_2}, \quad (19)$$

where ε_1 and ε_2 are the emissivities of the radiation surfaces. The conductivity of the argon gas, λ_{gas}, is temperature dependent and can be calculated as:

$$4.092 \cdot 10^{-4} \cdot T^{0.6748} \quad (20)$$

where T is the temperature of the material (Ikonen, et al., 2018). All the parameters used in calculating the effective heat conductivity are presented in Table 14.

Table 14. *Parameters for the effective heat conductivity.*

Parameter	Value	Source
Thermal conductivity of Ar-gas at 25 °C [W/(m·K)]	0.0191	calculated, equation 10
Thermal conductivity of Ar-gas at 60 °C [W/(m·K)]	0.0206	calculated, equation 10
Width of the gap [mm]	1.5	Mean of the gaps from Ikonen et al. (2018)
Surface emissivity of the inner radiation surface	0.6	(Ikonen, et al., 2018)
Surface emissivity of the outer radiation surface	0.1	(Ikonen, et al., 2018)
Total surface emissivity	0.09375	calculated, equation 9
Stefan-Bolzmann constant [W/(m^{2}K^4)]	$5.6697 \cdot 10^{-8}$	

The thermal conductivities of the buffer materials according to Ikonen et al. (2018) are used. The canister material thermal conductivities in the model are according to Raiko (2013) and the backfill material thermal conductivity according to Ikonen & Raiko (2012). The rock thermal conductivity used in Study 1 (verification of results) is the average thermal conductivity of the Olkiluoto area by Kukkonen (2015). The thermal conductivities of the materials are presented in Table 15.

***Table 15.** Thermal conductivities of host rock, buffer, backfill and canister materials in W/(m·K).*

Host rock		
Thermal conductivity at 25 °C	2.64	calculated, equation 7
Thermal conductivity at 60 °C	2.57	calculated, equation 7
Thermal conductivity used in study 1 verification	2.77	(Kukkonen, 2015)
Buffer		
Bentonite block conductivity at installation state	1.0	(Ikonen, et al., 2018)
Bentonite block conductivity in saturated condition	1.3	(Ikonen, et al., 2018)
Pellet conductivity at installation state	0.19	(Ikonen, et al., 2018)
Pellet conductivity at pre-wetted state	0.4	(Ikonen, et al., 2018)
Backfill material		
Backfill conductivity	1.6	(Ikonen & Raiko, 2012)
Canister materials		
Copper conductivity	391	(Raiko, 2013)
Cast insert conductivity	36.0	(Raiko, 2013)
Steel lid conductivity	57.5	(Raiko, 2013)
Argon gas effective conductivity at 25 °C	0.0213	calculated, Equation 8
Argon gas effective conductivity at 60 °C	0.0236	calculated, Equation 8

4.1.4 Initial temperatures

The initial temperatures are also needed for the simulations. According to Ikonen, et al. (2018) the thermal gradient in the Olkiluoto area is 1.3-1.4 °C /100 m. The ambient temperature at the disposal level is 10.5 °C. Accordingly temperature at top part of the block is set to 9 °C and at the bottom 13 °C in the model. Bentonite blocks and pellets share the same initial temperature as the surrounding rock. The temperatures of all the disposal canister materials are 50 °C at initial state. All initial temperatures are presented in Table 16.

***Table 16.** Initial temperatures of the disposal site.*

Parameter	Value	Source
Thermal gradient [°C /100m]	1.3-1.4	(Ikonen, et al., 2018)
Rock ambient temperature at disposal level [°C]	10.5	(Ikonen, et al., 2018)
Rock ambient temperature at top of the host rock [°C]	9	(Ikonen, et al., 2018)
Rock ambient temperature at bottom of the host rock [°C]	13	(Ikonen, et al., 2018)
Copper cylinder temperature at disposal [°C]	50	(Ikonen, et al., 2018)
Cast insert temperature at disposal [°C]	50	(Ikonen, et al., 2018)
Steel lid temperature at disposal [°C]	50	(Ikonen, et al., 2018)

4.1.5 Fuel Decay heat

The fuel decay heat acts as an external heat source Q in the Equation 3. The used fuel in this study is BWR type fuel with 40 MWd/kgU burn up. The fuel has been cooled for 32.30 years so that maximum canister power of 1700 W is reached (Ikonen, et al., 2018). The fuel decay heat is presented by Ikonen, et al. (2018 Appendix A Table A1 p. 100). The data is entered into COMSOL Multiphysics as a piecewise linear interpolation function.

4.1.6 Radiation parameters

The parameters used in the surface-to-surface module of COMSOL Multiphysics are presented in Table 17.

Table 17. *Parameters used in the radiation module.*

Parameter	Value	Source
Surface emissivity of copper	0.1	(Ikonen, et al., 2018)
Surface emissivity of steel lid	0.6	(Ikonen, et al., 2018)
Surface emissivity of cast iron	0.6	(Ikonen, et al., 2018)
Refractive index	1	
Radiation resolution	256	
Radiation method	Hemicube	

4.1.7 Boundary conditions

The boundary conditions for the Task 1 and Task 2 are as follows: The top and bottom part of the host rock block are set to fixed temperatures presented in Table 6. The host rock block is tall enough, for the thermal pulse not be affected by the boundary temperature. The vertical boundaries of the rock and canister surroundings are set to be symmetrical, meaning that the boundary condition is:

$$-\boldsymbol{n}\cdot\boldsymbol{q} = 0. \tag{21}$$

where $\boldsymbol{n}$ is the normal direction and $\boldsymbol{q}$ the heat flux. By setting the vertical boundaries symmetrical, the thermal effect of adjacent tunnels and canisters can be modelled without increasing the computational effort.

4.2 Task 3

4.2.1 Thermo-mechanical properties of the host rock

The thermo-mechanical parameters in the model are according to Posiva (2012) and are same as in the study by Hakala, et al. (2014). All the thermo-mechanical parameters of the host rock are presented in Table 19.

Table 19. *Thermo-mechanical properties of the host rock.*

Parameter		Source
Young’s modulus [GPa]	55	(Posiva, 2012)
Poisson’s ratio	0.25	(Posiva, 2012)
Coefficient of thermal expansion [1/°C]	$9.5\cdot10^{-6}$	(Posiva, 2012)

4.2.2 Failure parameters

The cohesion and internal angle of friction needed for the failure analysis are presented in Table 20.

Table 20. *Parameters needed for the failure criterion.*

Parameter		Source
Internal angle of friction in the repository area [º]	44	(Posiva, 2012)
Cohesion [MPa]	12.4	(Siren, 2011)

4.2.3 External stress tensor

According to Posiva (2012), the Olkiluoto disposal area rock can be split into three domains divided by Hydraulic (HZ) and Brittle Deformation Zones (BDZ). The disposal area lies in between HZ20 and BFZ099. In that domain the stress field is also affected by the vertical depth, marked by z in the Table 21.

Table 21. *The initial stresses of the repository area.*

	σ_H	σ_h	σ_v
Mean stress [MPa]	10.9+0.033z	5.3+0.027z	0.0265z
Orientation [ºN]	112	202	-

The external stress tensor $\boldsymbol{\sigma}_{\text{ext}}$ is then created form the in situ stresses:

$$\boldsymbol{\sigma}_{\text{ext}} = \begin{bmatrix} 10.9 + 0.033\text{z} & 0 & 0 \\ 0 & 5.3 + 0.027\text{z} & 0 \\ 0 & 0 & 0.0265\text{z} \end{bmatrix} [\text{MPa}]. \tag{22}$$

4.2.4 Boundary conditions

The boundary conditions are set such that they are compatible with the in situ stress. The top horizontal xy-face of the host rock block is set to be free to move in all directions. The bottom horizontal xy-face is set as a fixed constraint, that is $u = 0$. The vertical xz and xy faces are set to roller boundary condition, so that movement only in the z-direction is allowed, $\boldsymbol{u} \cdot \boldsymbol{n} = 0$.

Additionally the boundary load of the saturated bentonite is applied as a boundary condition to the tunnel and disposal hole walls. The boundary load is 5 MPa and its direction is towards the normal of the walls so that the positive direction is outwards.

5. Numerical model

5.1 Geometry

For Task 1, geometry and material properties presented in Chapter 3 and Chapter 4 are used. The disposal site is 100 m long in both the horizontal directions (xy-plane) to minimize the effect of any surrounding canisters. The heat source is modelled so that it is dependent on the vertical z-axis.

The data imported from Task 2 model into Task 3 model has to be mirrored in the horizontal x- and y-directions since in Task 2 symmetry is used to decrease the need of computational resources. The vertical z-axis coordinates have to be changed so that the coordinates of the imported data and the geometric model of Task 3 match. Additional data points in the y-direction have to be added to Task 2 thermal data, since in Task 3 the model geometry in y-direction is longer than in Task 2. The additional data points are added using Matlab by linear interpolation from the temperature data at Task 2 model geometry edge.

5.2 Solver

In COMSOL Multiphysics, Linear Lagrange type elements are used for spatial discretization of the thermal model. For the rock mechanical model, Quadratic serendipity elements are used. The thermal model is time dependent. The time dependent solver is adaptive order, adaptive step size backwards differentiation formula (BDF). The relative tolerance was set 5E-5 and Tolerance factor 0.1. The results are saved with an interval of 24 h. For the rock mechanical model a stationary solver is used, as the model is not time dependent. For both models, MUMPS direct solver is used as the linear system solver.

5.3 The mesh

In Task 1 and Task 2, the same mesh is used. The mesh is parametrized such that changing the disposal hole and tunnel spacing automatically scales the mesh. The element size in the argon gap for the 8.845 m disposal hole spacing in horizontal direction are approximately 0.5 mm · 9.3 mm · 45.0 mm.

In Task 1, the mesh consists of 127522 DOFs (degrees of freedom) and 560456 internal DOFs. In Task 2 with disposal hole spacing of 8.845, the mesh consist of 785478 DOFs and 2953586 internal DOFs. The mesh near the disposal canister in Task 2 is illustrated in Figure 5. For Task 3, a finer mesh is applied to the rock surrounding the disposal hole and tunnel. The mesh in Task 3consists of 492576 DOFs.

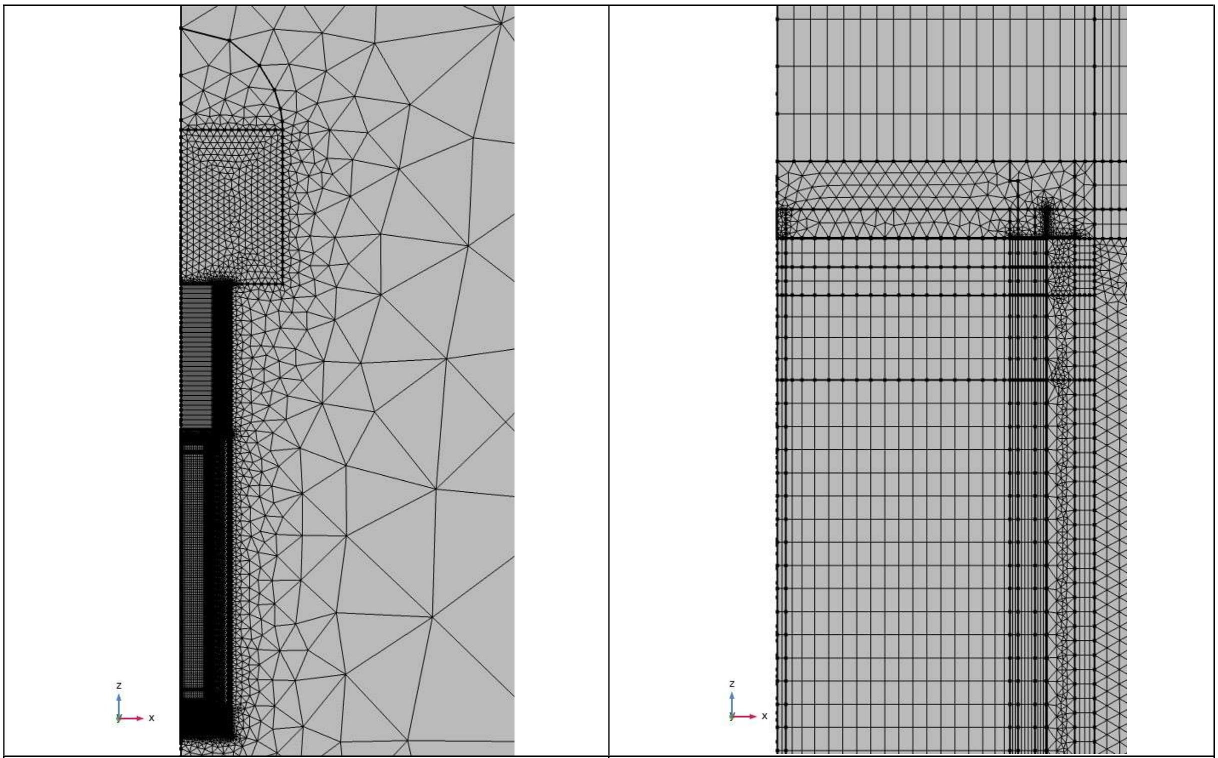

(a)	(b)

Figure 5. *(a) An illustration of the mesh on the xz-face. (b) A close-up figure of the same mesh near the disposal canister corner. The mesh is for the 8.845 m disposal hole spacing in Study 2.*

5.4 Radiation module settings

For the radiation method in COMSOL Multiphysics, *Hemicube* is used (COMSOL, 2018). Whit this radiation method shadowing is taken into account meaning for example that the radiation will not go through the corner in the argon gap in the model. The radiation resolution can be raised to increase the accuracy of the calculations with the cost of calculation time. For the refractive index, the default 1 (for vacuum) is used (COMSOL, 2018).

6. Results and discussion

6.1 Results of Task 1

The results of the first part of the Task 1 are compared to the results from Ikonen, et al. (2018) (Appendix B, Figure B3) in Figure 6. The maximum temperature calculated with the VTT in-house code (80.78 °C) is slightly higher than the calculated by Abaqus (both by Ikonen, et al. (2018)). The temperature calculated with the COMSOL Multiphysics model in this study is 0.08 °C higher than the temperature calculated with the VTT in-house code. With the scale in the upper graph, the temperature data between all models is very similar. The lower graph has been plotted in the near vicinity of the hottest temperature to better illustrate the differences in the maximum temperature.

The sensitivity of the highest temperature and its timing to rock thermal conductivity is studied by changing the rock thermal conductivity from the function by Ikonen, et al. (2018), Equation 17, to a constant average value (2.77 W/(m·K) at 25 °C) according to Kukkonen (2015). The difference between the thermal conductivities at 25 °C when comparing the aforementioned values is approximately 5%.

The highest temperature in the COMSOL model with the same heat conductivity of the rock as by Ikonen, et al. (2018) is 80.9 °C, which is reached 33.8 years after they have been taken out from the nuclear reactor. With the rock heat conductivity by Kukkonen (2015) the maximum temperature is 79.6 °C, which is reached 0.1 a earlier. The difference in the maximum temperature using the two heat conductivities is 1.3 °C (Table 22).

The change of 4.7% in the rock thermal conductivity leads to an over ten times larger difference in the highest temperature than the difference between the three simulation software. Therefore, it could be said that the results between the different software coincide.

Table 22. *Results of the validation study.*

	temperature [°C]	time [a]
Maximum temperature with temperature dependent rock conductivity	80.9	33.8
Maximum temperature with rock conductivity of 2.77 W/(m·K)	79.6	33.7

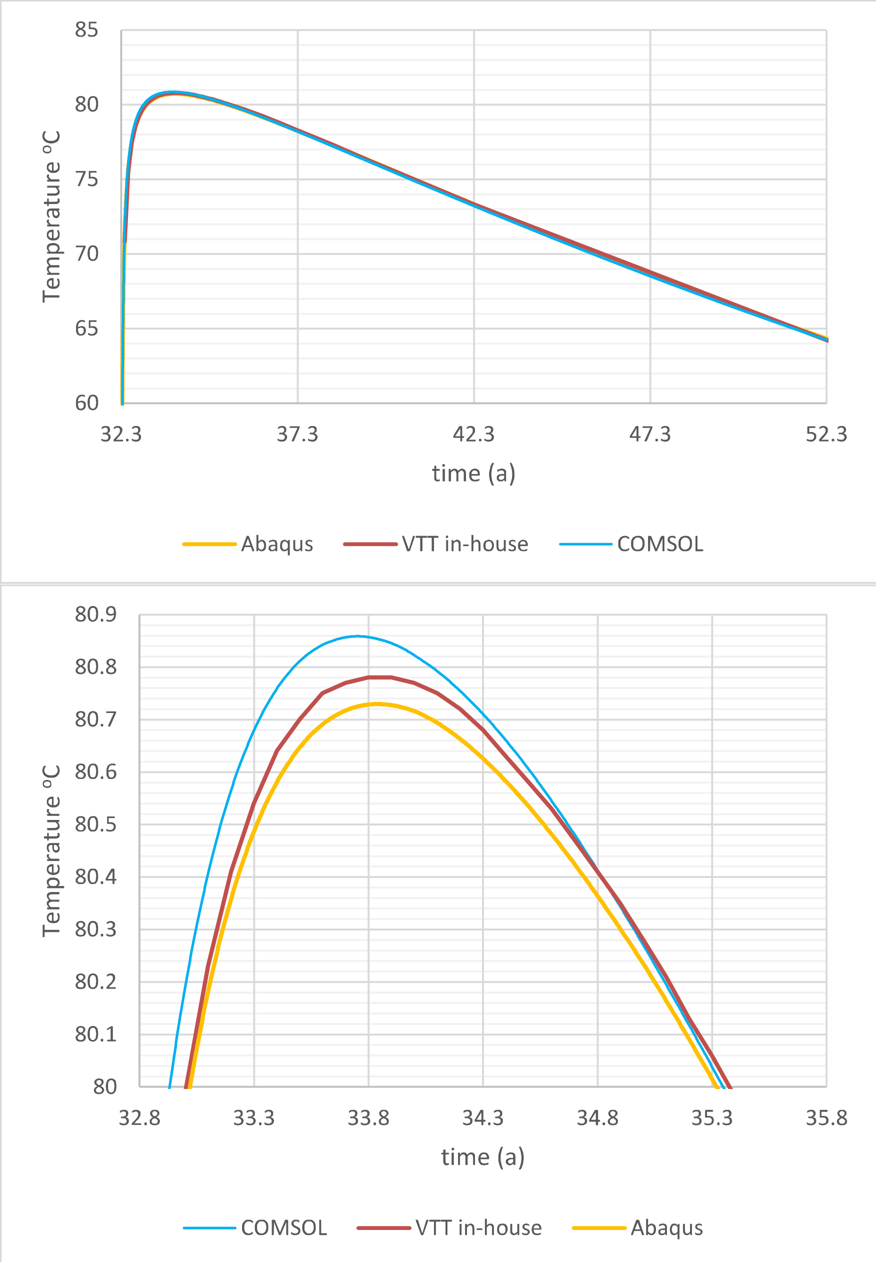

Figure 6. *The temporal evolution of temperature simulated with Abaqus (Ikonen, et al., 2018), VTT in-house code (Ikonen, et al., 2018) and COMSOL Multiphysics (this study). The zero time is when the nuclear fuel has been taken out from the nuclear reactor. The host rock surrounding the SNF-canister is 100 m long in all spatial directions. Note the scale.*

6.2 Results of Task 2

The results obtained in Task 2 differ from the results of Ikonen, et al. (2018) ranging from 0.1 to 1.0 °C. Table 23 presents the maximum temperatures calculated in Task 2 for tunnel spacing of 25 m, 30 m, 35 m and 40 m. The temperatures calculated by Ikonen, et al. (2018) are in brackets. The temperature distribution is presented in Figure 7.

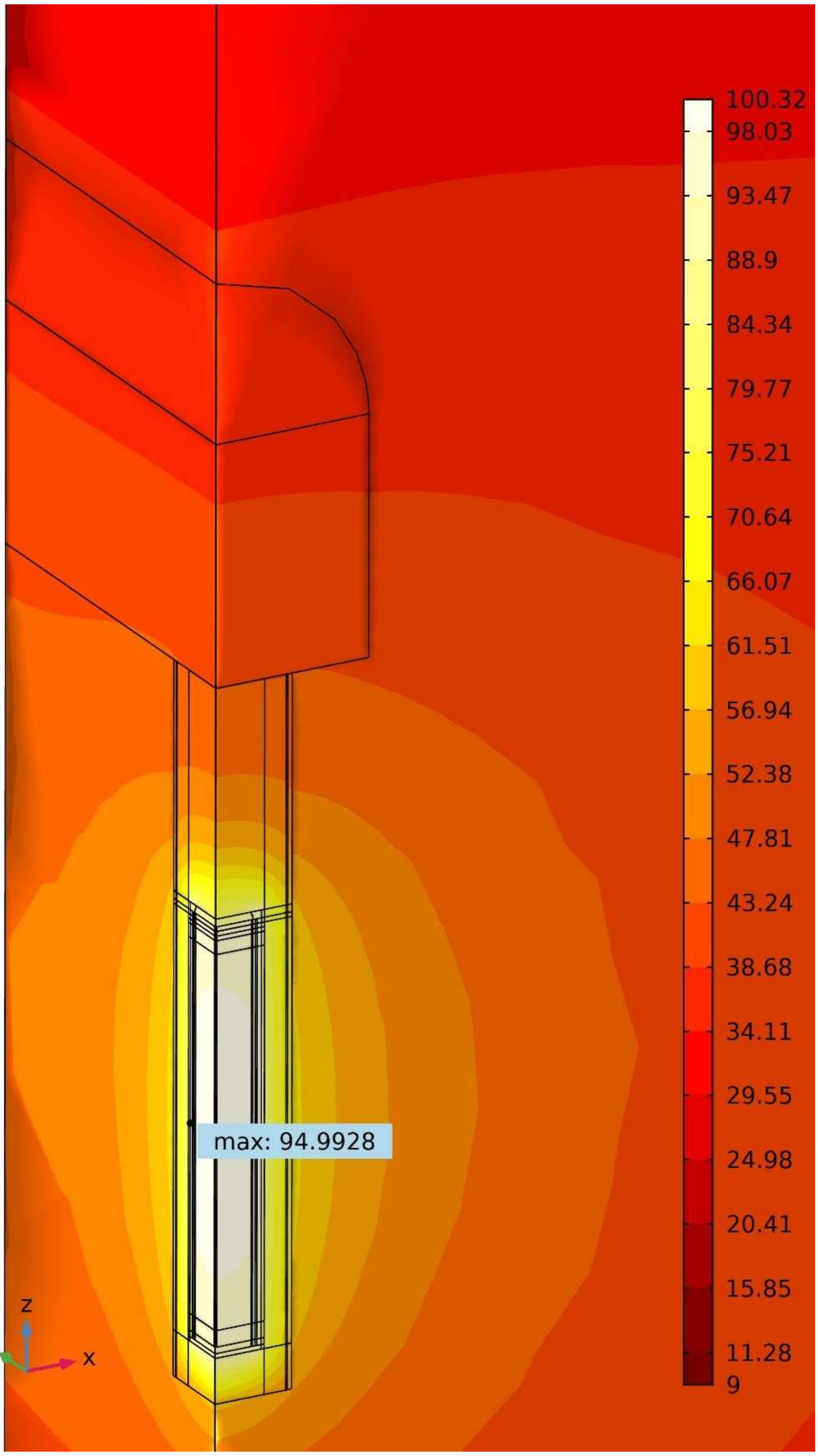

Figure 7. *Temperature field in the disposal area at the hottest time point in °C.*

Table 23. *Maximum temperature (°C) with various tunnel and disposal hole spacing. The values in brackets are by Ikonen, et al. (2018)*

Canister spacing (m) \ Tunnel spacing (m)	25	30	35	40
6	113.321, (112.91)	106.480, (106.61)	102.522, (102.61)	100.294, (100.54)
7	104.838, (104.66)	99.433, (99.65)	96.4159, (96.65)	94.7745, (95.11)
8	98.856, (98.82)	94.505, (94.88)	92.1753, (92.49)	91.0272, (91.42)
9	94.3585, (94.56)	90.884, (91.49)	89.0174, (89.58)	88.2125, (88.81)
10	91.1608, (91.46)	88.301, (89.00)	86.9089, (87.50)	86.2899, (86.89)
11	88.6838, (89.13)	86.334, (87.17)	85.1884, (85.91)	84.7727, (85.48)
12	86.7945, (87.34)	84.8781, (85.77)	84.0676, (84.72)	83.7599, (84.43)
13	85.3974, (85.96)	83.7546, (84.70)	83.1428, (83.83)	82.9268, (83.61)
14	84.2443, (84.88)	82.9264, (83.86)	82.4633, (83.15)	82.3180, (82.95)
15	83.3760, (84.04)	82.2828, (83.23)	81.9076, (82.59)	81.8095, (82.44)
16	82.7160, (83.36)	81.8014, (82.74)	81.4925, (82.15)	81.3924, (82.03)
17	82.1310, (82.81)	81.4092, (82.33)	81.1534, (81.80)	81.1516, (81.71)
18	81.7848, (82.38)	81.1291, (82.00)	80.9368, (81.53)	80.9231, (81.46)
19	81.3826, (82.05)	80.8878, (81.74)	80.7069, (81,31)	80.6714, (81.26)
20	81,1244, (81.77)	80.6782, (81.53)	80.5746, (81.15)	80.5131, (81.10)

The results obtained for 25 m tunnel spacing differ in between 0.04 - 0.7 °C from the result of Ikonen, et al. (2018). The smallest difference is near the tunnel length where the maximum temperature of 95 °C is reached. The difference between the studies is explained mainly due two factors. Firstly, a homogenized heat source is used in Study 2 without a vertical heat distribution. Secondly, the geometry in this study is assumed to be in the center of an infinite panel, where all the disposal canisters have been disposed simultaneously. The results are however very close to the original results, which will be sufficient for thermal stress analysis of Study 3.The absolute differences of all tunnel spacing are presented in Table 24.

Table 24. *Absolute difference of the maximum temperatures (°C) when comparing the results between this study and the study by Ikonen, et al. (2018).*

Canister spacing (m) \ Tunnel spacing (m)	25	30	35	40
6	-0.41	-0.13	-0.09	-0.25
7	-0.18	-0.22	-0.23	-0.34
8	-0.04	-0.38	-0.31	-0.39
9	0.20	-0.61	-0.56	-0.60
10	0.30	-0.70	-0.59	-0.60
11	0.45	-0.84	-0.72	-0.71
12	0.55	-0.89	-0.65	-0.67
13	0.57	-0.95	-0.69	-0.68
14	0.64	-0.93	-0.69	-0.63
15	0.66	-0.95	-0.68	-0.63
16	0.64	-0.94	-0.66	-0.64
17	0.68	-0.92	-0.65	-0.56
18	0.60	-0.87	-0.59	-0.54
19	0.67	-0.85	-0.60	-0.59
20	0.53	-0.85	-0.58	-0.59

The minimum canister spacing is determined for the tunnel spacing of 25 m. The result is obtained by changing the disposal hole spacing and pinpointing the spacing, where the temperature is not exceeded. The results presented in the Table 25. In the study of Ikonen, et al. (2018) the canister spacing where the temperature is maximally 95 °C is 8.88 m when the tunnel spacing is 25 m. The spacing according to Task 2 simulations is 8.85 m. The difference between the spacing is only 0.03 m.

Table 25. *Evaluating the disposal hole spacing with 25 m tunnel spacing. Green colour indicates the smallest disposal hole spacing where the temperature limit of 95 °C is not reached.*

	temperature [°C]	time [a]
parameter 8.8	95.15	46.8
parameter 8.83	95.07	46.717
parameter 8.84	95.01	46.717
parameter 8.845	94.99	46.717
parameter 8.85	94.98	46.717
parameter 9.0	94.36	48.717

6.2.1 Effect of the surface-to-surface radiation module

Instead of the effective conductivity in the argon gap, the second part of the Task 2 uses COMSOL surface-to-surface radiation module to model radiative heat transfer over gap. The calculation was conducted with tunnel spacing of 8.845 m, which yielded a temperature of 94.7777 °C. The temperature decreased 0.21 °C. The difference is negligible if compared to parameter sensitivity and the difference between different simulation software.

6.3 Results of Task 3

6.3.1 Stress state

In Task 3 two cases were studied. In the reference case, the disposal area is in a state, where the disposal tunnel is extracted from the host rock. The heat of the SNF-canister is not taken into account, but the buffer is assumed to be fully water saturated, causing a swelling pressure on the surrounding rock.

In the hot case the heat of SNF-canister is taken into account and the temperature of the host rock has reached its hottest point. The maximum temperature of the host rock is reached exactly 38 years after deposition and it is 67.7 °C. That is later than the maximum temperature of the bentonite, as it takes some time for the heat to transfer through the bentonite buffer.

In the reference case, the highest von Mises stress is 52.7 MPa. In Case 2 the highest von Mises stress is 121.5 MPa. The maximal von Mises stress increases by 68.8 MPa from the reference case to the hot case. It is worth noting, that the highest stress is located near the corner between the tunnel floor and walls and is only affecting a very narrow area. If the stress is analyzed outside corner areas, the highest von Mises stress is 73.1 MPa and it is located in the disposal hole wall. The von Mises stress distributions of both cases are presented in Figure 8.

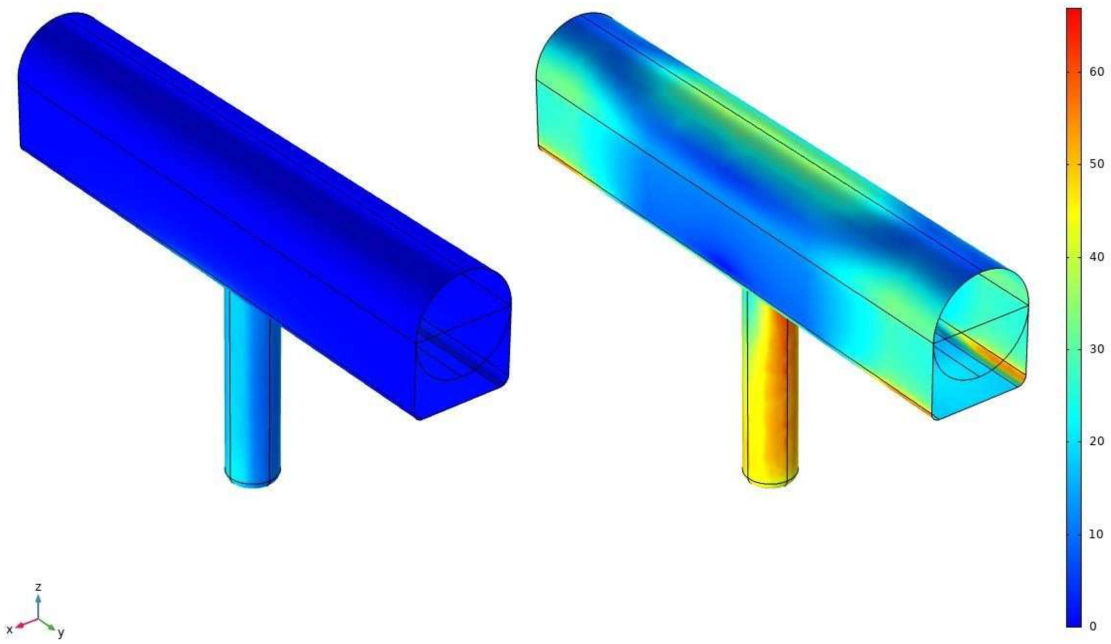

Figure 8. *von Mises stress of a tunnel section with one disposal hole. The cold case is illustrated the left and the hot case on right. The units in the colour legend are in MPa.*

Posiva conducted an experiment called POSE Phase 2 (Valli, 2014), where an area of rock was heated with external heaters in the disposal area. In that study, two vertical holes, which are very close to each other are studied. The rock reached a temperature of over 68 °C, which caused the principal stress to exceed 130 MPa near the walls of the disposal hole.

In the COMSOL Multiphysics model, the highest thermally induced stress is located in the elements in the sharp corners of the tunnel geometry. Outside the sharp corners of the geometry, the highest von Mises stress is 121.5 MPa. The highest von Mises outside the sharp corners differs slightly from the results of Valli (2014), but the difference can be explained with different geometries of the studied sites. The heating in POSE Phase 2 also occurs very fast compared to the heating in the COMSOL model, and thereby the temperature gradient in the rock in POSE Phase 2 is larger.

6.3.2 Failure analysis

Posiva (2012) proposes a rock strength model for the disposal area. The model is based on a uniaxial compression test. The model states a crack initiation stress (CI) and crack damage stress (CD). If the CI stress is exceeded, damage begins in the rock. Crack damage strength is the true peak strength of the rock. Values for CI and CD are presented in Table 27.

Table 27. *Rock strength parameters.*

Parameter		source
Crack initiation strength [MPa]	52	(Posiva, 2012)
Crack damage strength [MPa]	99	(Posiva, 2012)

When the values of Posiva (2012) are compared to the values of the COMSOL model it can be seen that the von Mises stress in the Case 2 exceed the CI strength in the disposal hole and the sharp corners of the tunnel floor (Figure 9).

The rock failure in the COMSOL model was also analyzed using the Drucker-Prager failure criterion, described in Chapter 4.3.4. The analysis shows, that the failure criterion is exceeded in the disposal hole wall and tunnel bottom corner area. The areas, where the failure criterion is exceeded are presented in Figure 10.

Both failure analyses show similar results. The failure criterions are exceeded in the disposal hole and the sharp tunnel corners. In the Drucker-Prager analysis, the yield criterion is additionally met in the roof of the tunnel.

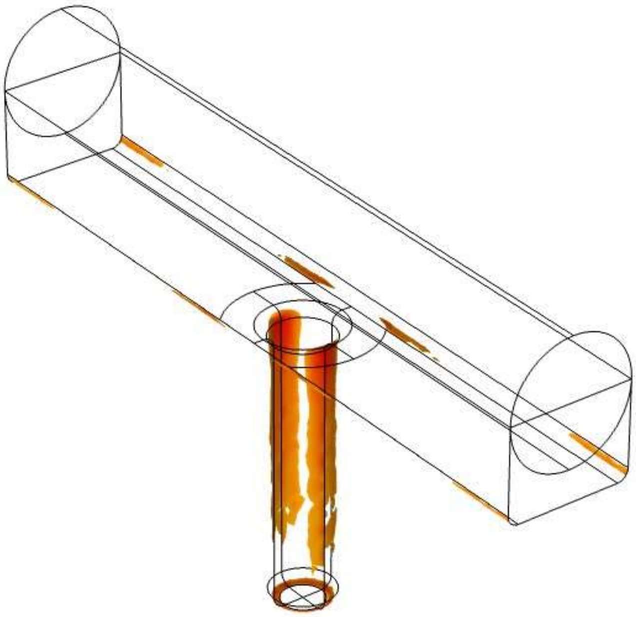

Figure 9. *Disposal hole and tunnel locations where the von Mises stress exceeds the crack initiation strength. These areas undergo plastic deformation.*

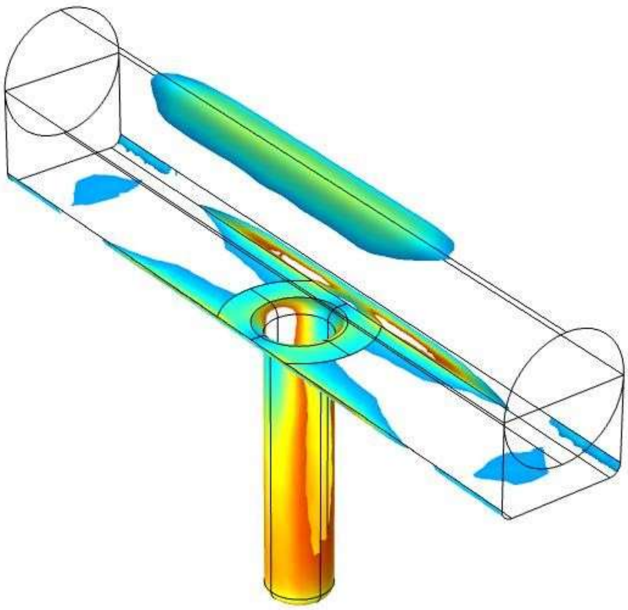

Figure 10. *The locations, where the Drucker-Prager failure criterion is exceeded are plotted on the tunnel surface.*

The results are in line with the results from a study conducted by Hakala, et al. (2014). There are differences between the studies with the most significant being that in the COMSOL model has only an area consisting of a single disposal tunnel with one disposal hole is studied. The general results should be still comparable. The study by Hakala, et al. (2014) showed, that the temperature increment causes the stress state to rise above the CI stress in many areas of the repository.

The Pose experiment showed that the CI stress is exceeded over 45 cm deep into the rock (Valli, 2014). In the COMSOL model, the von Mises stress only exceeds the CI very close to the bentonite surface. The Drucker-Prager criterion is however exceeded deeper into the rock. Figure 11 shows that the criterion is exceeded almost 1 m deep. The 2D-slices are evaluated from the middle of the canister on the xy-plane.

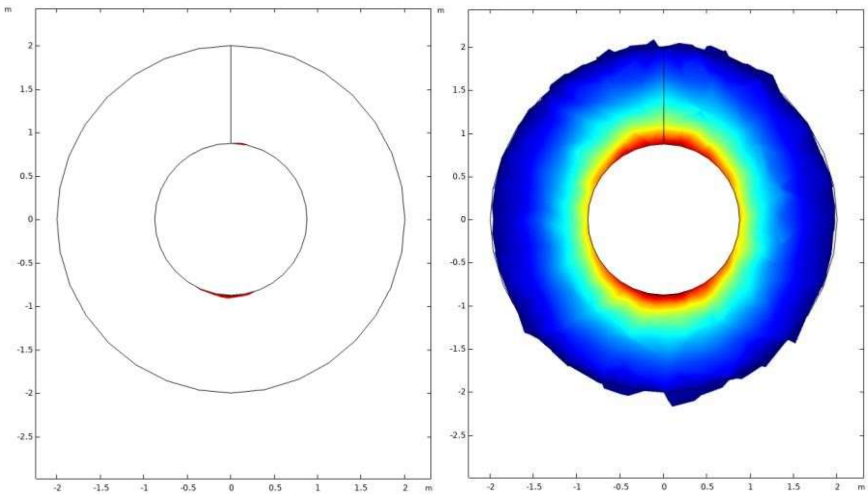

Figure 11. *The areas, where the failure criterion are exceeded. Crack initiation strength is plotted on the left and Drucker-Prager on the right.*

7. Conclusions

In this study, a COMSOL Multiphysics heat transfer model for the SNF repository was successfully created. The model is capable of reproducing existing simulations of the disposal area temperature with good precision. The model proved to be a useful tool for analyzing the thermally induced stress in the disposal area. In the future, the verified model can be utilized in 1) scoping the thermal conditions of the disposal site for experiments and 2) developing thermally coupled models with a flexible simulation software.

In Task 1, the model by Ikonen, et al. (2018) was recreated to verify the results of the COMSOL Multiphysics model. The results calculated in Task 1 were compared to the results calculated with Abaqus and VTT in-house code. Additionally the same study was conducted with a different rock heat conductivity proposed by Kukkonen (2015) to see if a small difference (5%) in rock thermal conductivity causes a larger difference in results than the difference between Task 1 results and those by Ikonen, et al. (2018). The maximum difference between Task 1, and VTT in-house code was 0.08 °C, which was significantly smaller than the difference caused by different heat conductivities (1.3 °C)

In Task 2 the transfer of the decay heat from the SNF-canisters to the surrounding buffer and rock was calculated. The disposal hole spacing was varied between 6 m to 20 m and the tunnel spacing between 25 m, 30 m, 35 m and 40 m. The minimum allowed disposal hole distance (with temperature below 95 °C) for 25 m tunnel spacing was calculated (8.845 m) which is very close to the results by Ikonen, et al. (2018) (8.88 m). Additionally the effect of a more accurate radiation model over the argon gap between the copper over pack and cast insert was studied. The more accurate radiation model decreased the maximum temperature by 0.2 °C, which is small change in comparison to the parameter uncertainty.

In Task 3 the effect of thermal evolution of the rock on its stress state was studied. Task 3 was divided to two cases. The first case was the reference case, where only the in-situ stress and the swelling pressure of saturated bentonite was applied on the backfilled disposal geometry. In the second case, stress caused by the thermal expansion of the rock due to the decay heat was studied. The highest thermally induced stresses were located in the disposal hole and the corners of the disposal tunnel floor. On those locations, the failure criterion was exceeded. The failure analysis using Drucker-Prager yield criterion shows that the damaged rock area could continue 1 m deep into the rock. Damage in the area is important to factor in, because fractures in the area can increase ground water flow near the disposal canister. In the case of a canister failure, it can speed up the transport of radionuclides (Poteri, et al., 2014).

References

Alejano, L.R., Bobet, A., 2012. Drucker–Prager Criterion. Rock Mech Rock Eng 45, 995-999. https://doi.org/10.1007/s00603-012-0278-2

Brady, B.H., Brown, E., 2007. Rock Mechanics, 3rd. ed. ed. Springer Science & Business Media, Dordrecht.

COMSOL, 2018. Heat Transfer Module User's Guide [WWW Document]. COMSOL. URL https://doc.comsol.com/5.4/doc/com.comsol.help.heat/HeatTransferModuleUsersGuide.pdf (accessed 9.2.2019).

Engineering ToolBox, 2019. Gases - Densities [WWW Document]. Engineering ToolBox. URL https://www.engineeringtoolbox.com/gas-density-d_158.html (accessed 9.2.2019).

Hakala, M., Ström, J., Nujiten, G., Uotinen, L., Siren, T., Suikkanen, J., 2014. Thermally Induced Rock Stress Increment and Rock Reinforcement Response. Posiva OY, Eurajoki.

Hakala, M., Valli, J., 2014. ONKALO POSE Experiment – Phase 1 & 2: 3D Thermo-Mechanics Prediction. Posiva Oy, Eurajoki.

Hökmark, H., Lönnqvist, M., Kristensson, O., Sundberg, J., Hellström, G., 2009. Strategy for thermal dimensioning of the final repository for spent nuclear fuel. Svensk Kärnbränslehantering AB, Stockholm.

Ikonen, K., 2005. Thermal Analysis of Repository for Spent EPR-type Fuel. Posiva OY, Eurajoki.

Ikonen, K., Kuutti, J., Raiko, H., 2018. Thermal DImensioning for the Olkiluoto Repository - 2018 Update. Posiva OY, Eurajoki.

Ikonen, K., Raiko, H., 2012. Thermal Dimensioning of Olkiluoto Repository for Spent Fuel. Posiva, Eurajoki.

Ikäheimonen, T.K., 2002. Säteily ja sen havaitseminen. Säteilyturvakeskus, Hämeenlinna.

Keto, P., Hussan, M.M., Karttunen, P., Kiviranta, L., Kumpulainen, S., Korkiala-Tanttu, L., Koskinen, V., Jalonen, T., Koho, P., Sievänen, U., 2013. Backfi ll Production Line 2012 Design, Production and Initial State of the Deposition Tunnel Backfi ll and Plug. Posiva Oy, Eurajoki.

Kukkonen, I., 2015. Thermal Properties of Rocks at Olkiluoto: Results of Laboratory Measurements 1994-2015. Posiva Oy, Eurajoki.

Markku, J., 2013. BUFFER DESIGN 2012. Posiva Oy, Eurajoki.

Posiva Oy, 2012. Olkiluoto Site Description 2011. Posiva Oy, Eurajoki.

Poteri, A., Nordman, H., Pulkkanen, V.-M., Smith, P., 2014. Radionuclide Transport in the Repository Near-Field and Far-Field. Posiva Oy, Eurajoki.

Raiko, H., 2013. CANISTER DESIGN 2012. Posiva Oy, Eurajoki.

Raiko, H., 2005. Disposal Canister for Spent Nuclear Fuel – Design Repor. Posiva Oy, Eurajoki.

Saanio, T., Ikonen, A., Keto, P., Kirkkomäki, T., Kukkola, T., Nieminen, J., Raiko, H., 2013. Design of the Disposal Facility 2012. Posiva Oy, Eurajoki.

Siren, T., 2011. Fracture Mechanics Prediction for Posiva's Olkiluoto Spalling Experiment (POSE). Posiva Oy, Eurajoki.

Valli, J., 2014. *ONKALO POSE Experiment – Phase 1 & 2: 3D Thermo-Mechanics Prediction,* Eurajoki: Posiva Oy.